CARBON 69 (2014) 390–400

Available at www.sciencedirect.com

ScienceDirect

journal homepage: www.elsevier.com/locate/carbon

A blister test for interfacial adhesion of large-scale transferred graphene

Z. Cao [a], P. Wang [a], W. Gao [a], L. Tao [b], J.W. Suk [c], R.S. Ruoff [c], D. Akinwande [b], R. Huang [a], K.M. Liechti [a,*]

[a] Department of Aerospace Engineering and Engineering Mechanics, Research Center for the Mechanics of Solids, Structures and Materials, The University of Texas at Austin, Austin, TX 78712, United States

[b] Department of Electrical and Computer Engineering, The University of Texas at Austin, Austin, TX 78712, United States

[c] Department of Mechanical Engineering and The Materials Science and Engineering Program, The University of Texas at Austin, Austin, TX 78712, United States

ARTICLE INFO

Article history:
Received 31 August 2013
Accepted 13 December 2013
Available online 25 December 2013

ABSTRACT

A blister test and associated analysis was developed to characterize the interfacial adhesion between graphene and substrates to which it has been transferred. In this study, chemical vapor deposition grown graphene had been transferred to a highly polished copper substrate from its seed foil. The graphene/photoresist composite film was pressurized with deionized water through a nominally 1-mm hole in the copper and the deflection of the membrane was measured by a full field interference method. The deflection profiles compared well with those obtained from a linear plate model that accounted for the initial strain in the membrane and a relaxed boundary condition at the edge of the blister. This was used to calculate the energy release rate as a function of delamination growth to obtain fracture resistance curves for the graphene/copper interface. To the best of our knowledge, these are the first measurements of fracture resistance curves for adhesive interactions between transferred graphene and a copper substrate. The delamination path of the graphene/photoresist sample was confirmed by Raman spectroscopy. The measured adhesion energy for the graphene/copper interface was higher than that of a photoresist/copper interface, but slightly lower than previous measurements for as-grown graphene on copper foil.

1. Introduction

Graphene is a one-atom thick layer of carbon atoms arranged in a regular hexagonal pattern. The Young's modulus and intrinsic strength of graphene were first measured by Lee et al. [1] as 1 TPa and 130 GPa, respectively. Based on its electronic and thermal transport, optoelectronic and mechanical properties, many potential applications of graphene have been proposed and demonstrated. Simply as a few examples, high frequency graphene transistors (100 GHz) have been reported [2], and its high flexibility and possibly high strength (as yet unproven at macroscale) suggest graphene as a candidate to replace indium tin oxide (ITO) in transparent conductive film applications, particularly in flexible systems [3]. In almost every application, high quality monolayer graphene in controllable sizes is needed.

Various methods have been proposed to produce large area, monolayer graphene. Among them, one of the most

* Corresponding author.
E-mail address: kml@mail.utexas.edu (K.M. Liechti).
0008-6223/$ - see front matter
http://dx.doi.org/10.1016/j.carbon.2013.12.041

promising is chemical vapor deposition (CVD). Li et al. [4] grew large area monolayer graphene on copper foil. Growth on nickel and ruthenium thin films have also been reported [5,6] (among many other substrates that have been studied by surface scientists under UHV growth conditions [7]). For scaled applications graphene would thus be grown on one substrate and then transferred to a target substrate or perhaps used as a membrane; this motivates determining the adhesive properties of graphene in order to design for or otherwise facilitate successful transfer, as well as for achieving fundamental scientific understanding. Several experiments have been carried out to measure the adhesion energy of graphene on various substrates. By intercalating nanoparticles between graphene and silicon, Zong et al. [8] reported the adhesion energy to be 0.151 J/m^2. Koenig et al. [9] measured the adhesion of micromechanically exfoliated graphene on SiO_2, finding 0.45 J/m^2 for monolayer graphene and 0.31 J/m^2 for two to five layer graphene. The various adhesion energies obtained might be due to contamination, surface roughness, or liquid trapped between graphene and the substrate. Yoon et al. [10] used double cantilever beams (DCB) to measure the adhesion energy of graphene as-grown on copper at 0.72 J/m^2, which is notably higher.

The blister test is a well-known method to measure adhesion of thin films to their substrate as stress concentrations are avoided by the application of a uniform pressure. Hinkley [11] was among the first to use this method. Other pioneering works include: Gent and Lewandowski [12] who studied initiation and subsequent delamination of thin films; Liechti and Hanson [13] who examined nonlinear effects in blister testing; Liechti and Shirani [14] who developed an analysis for blisters having a wide range of thickness and established when plastic yielding was dominant. Because adhesion plays an important role in the field of microelectronics, many experiments have been performed on small scale blisters [15–17]. Using a volumetric measurement, Hohlfelder et al. [18] extracted the adhesion energy of SiN_x on silicon substrates. Yahiaoui used an interferometric system to investigate the deformation of micro-machined films [19]. Some theoretical efforts include the work by Jensen [20] who studied the effect of mode-mix due to the different properties of the film and the substrate; Shirani and Liechti who accounted for interactions between the film and substrate by cohesive zone modeling [21,22] with calibrated traction–separation relations; Wang et al. [23] who studied the effect of van der Waals interactions between graphene and the substrate.

In this study, we present a series of blister tests for photoresist and photoresist/graphene composite membranes placed on a copper substrate. Full field interferometry measurements were carried out to measure the blister profiles. The effects of the pre-strain and the boundary condition at the delamination front were taken into account for data analysis. This allowed the fracture resistance curves associated with the graphene/copper and photoresist/copper interfaces to be determined, from which the corresponding adhesion energies were obtained. Raman spectroscopy was used to identify the delaminated interface and potential fracture mechanisms were discussed based on all these results.

2. Experimental

In this section, we describe the experimental components that were developed for this work. These include apparatus, specimen preparation, image and data processing.

2.1. *Apparatus*

Fig. 1 is a schematic of the apparatus, which consisted of a syringe pump, a pressure transducer, an optical microscope and a computer data acquisition system. A syringe pump (NewEra Pump Systems Inc., NE500) with a high pressure syringe (5 ml Antron Engineering & Machines) was used to apply pressure under nominally volume control. It was guaranteed to be leak-free up to 5 MPa. The flow rate of the syringe pump ranges from 20 μl/h to 500 ml/h with an accuracy of 0.5%. To maximize the stiffness of the system, all the connecting components were as short as possible. After filling the system with deionized water, trapped air bubbles were minimized in order to further increase the stiffness of the system. These steps were all taken with a view to increasing the stability of delamination and postpone the transition to fast separation of the membrane. Another major issue with trapped air arises when the measurement of the blister height is based on the volume of water injected [18]. However, in our experiment, this issue was avoided by determining the height directly by optical interference.

A pressure transducer was used to measure the pressure on the blister. The pressure transducer (Sensotec Z/0761-09ZG) had a resolution of 0.2% and a range of 344 kPa. The transducer signal was recorded by a computer data acquisition system which consisted of a PC with LabVIEW software and a data acquisition board (National Instruments PCI-MIO-16XE-50).

An optical microscope (Olympus BX41M) equipped with a 5× Michelson interferometer objective (Nikon, CF IC EPI PLAN TI 5X) was used to measure the blister deformation *in situ*. A digital camera (Lumenera, Infinity3-1M) recorded fringe patterns every 10 s. The objective had a depth of field of 7 μm and the microscope/camera system had a spatial resolution of 1.5 μm. The specimen was illuminated by green light (550 nm). The tests were conducted in the ambient laboratory environment at 22 °C and a relative humidity of 33%, which can be considered to be quite benign for the photoresist.

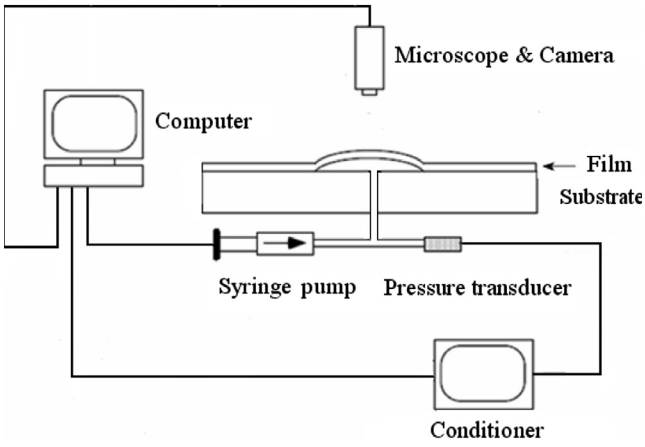

Fig. 1 – Schematic of blister test apparatus.

2.2. Specimen preparation

In this study we were interested in determining the adhesion of monolayer graphene that had been transferred to copper. Accordingly, two types of specimens were considered. First was a composite film of graphene coated with an epoxy photoresist SU-8 2025 (MicroChem Corporation). The purpose of the photoresist was to facilitate transfer of the graphene to the copper and reinforce it during pressurization. For comparison, the second specimen consisted of the same photoresist on copper but without graphene.

The graphene that was used in this study was produced by chemical vapor deposition (CVD), the details of which can be found in [4,24]. The preparation of the photoresist started with depositing a copper layer, roughly 100 nm thick, on a silicon wafer using a Denton thermal evaporation system. The operating pressure was approximately 10^{-6} Torr and the deposition rate was 1 Å/s. The photoresist was spun on top of the copper layer at 2500 rpm for 35 s. The nominal thickness of the photoresist was 33 μm, but this was measured in each experiment using a profilometer (Dektak6M) with a vertical range and resolution of 260 μm and 10 nm, respectively. The sample was then soft-baked at 80 °C for 5 min. A razor blade was used to cut grids of 1×1 cm on the photoresist membrane. Then the assembly was submerged in an ammonium persulfate solution (1.0 wt.%). The etchant flows through the trenches to etch away the copper underneath the photoresist. This process took 3–4 h. Finally, all the small squares of photoresist were sonicated in deionized water. In this way, optically flat photoresist films were obtained and each square was used to produce a circular blister on copper.

The membranes consisting of graphene coated with photoresist were prepared in the same fashion except that a monolayer of CVD graphene was first transferred to the same copper on silicon substrate referred to above [25,26]. The photoresist was applied, cured and diced as above to produce squares of graphene/photoresist. The etching process did not adversely affect the adhesion of graphene to the photoresist.

The next step was to transfer the membrane over a 0.797 mm diameter drilled hole in a copper substrate to produce a free-standing window. The copper substrate was made of 101 oxygen-free, high-conductivity (OFHC) copper (Trident, Inc.). The surface of the substrate was first polished by a range of sand papers, then by 3 μm, 1 μm, and 0.05 μm diamond compound pastes, until it was mirror-like. Fig. 2 displays the topography of the copper substrate obtained by atomic force microscopy (AFM). The root-mean-squared (RMS) roughness was 4.7 nm over a 10×10 μm area approximately 0.15 mm from the edge of the hole. The RMS roughness of three other areas nearby was 4.4, 4.1, and 3.9 nm. Deionized water and acetone were applied to clean the surface after polishing.

After the transfer, the specimen was baked at 135 °C for 15 min with pressure being applied via a small weight (approximately 100 g). The weight prevented the heat flux from blowing off the membrane, and also improved the contact between the membrane and the substrate. The graphene with photoresist sample was prepared in a similar fashion, making sure that the graphene side was in contact with the copper.

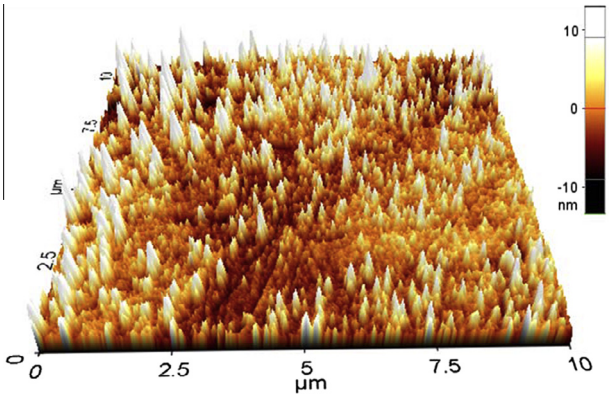

Fig. 2 – An AFM image of the topography of the copper substrate. The RMS roughness is 4.7 nm over an area of 10×10 μm^2. (A color version of this figure can be viewed online.)

2.3. Blister deflection

After attaching the specimen to the pressure manifold with a rubber O-ring seal, it was placed under the microscope (Fig. 1). The distance between the objective and the specimen was carefully adjusted so that fringe patterns were visible. At this time the tilt of the reference mirror in the interference objective was also adjusted to establish proper alignment. At zero pressure, the free-standing membrane was slack and drooped below the copper substrate. The reason for this is not clear, but one possibility is that gravity pulled the membrane down while the epoxy was softening during the baking. Van der Waals interactions between the films and side wall have been noted for suspended graphene [9], but it is unlikely that they were the cause of this phenomenon here due to greater thickness of the films. Another possibility is that the application of the weight at 135 °C to enhance contact following transfer resulted in compressive residual strains during cool down. At the same time, the glass transition temperature of the photoresist is 200 °C, making it unlikely that large viscoelastic effects could be responsible for this. Deflection profiles in this initial state were obtained. In subsequent analysis of these profiles, deflections were measured with respect to this initial state. As the pressure increased due to the injection of deionized water at a rate of 5 ml/h, a number of phenomena were observed. More and more circular fringes were generated, as the membrane was pressurized. Stable delamination of the blister from the substrate initiated at a critical pressure (approximately 75 kPa). In this regime, the delamination could be arrested by stopping injection and the delamination front remained quite circular. This is indicative of uniform adhesion. The stable growth took place over about 50 μm and was followed by unstable crack growth and blow-off of the membrane. Before the blow-off, the delamination propagated rapidly for approximately 2 s. Stopping injection did not arrest the propagation. During the whole process, distinguishable fringes were apparent all over the blister, thereby enabling whole field measurement of the blister deflections. The membrane thickness was optimized to make sure that the full range of deflections could be measured within the

range of the pressure transducer. Membranes having a nominal thickness of 33 μm achieved this objective.

Images of the fringe patterns were taken at 10 s intervals using a time-lapse recording feature of the camera. The membrane deflections were extracted from the centerlines of the dark fringes. The associated image processing was accomplished with the ImageJ application. First, the image was divided into approximately 30 square regions which were chosen so that, within each region, the contrast of the dark and bright fringes was roughly the same. Then the brightness and contrast of each region was optimized until the "finding local maximum" feature of ImageJ generated centerlines of the dark fringes. Since the optimization of brightness and contrast depended mainly on human judgment, which could be a source of error, this operation was carried out several times on the same photo to examine reproducibility. The difference was minimal. Finally, all the square regions were assembled according to their locations in the original gray-scale photo and the centerlines of the fringes were extracted for subsequent transformation to the blister profiles.

Fig. 3a is the interferogram of a blister at 88.3 kPa. The diameter of this blister was 0.797 mm. Each fringe represents a height contour. For these experiments, the height interval between two successive dark fringes was 275 nm ($\lambda/2$). The corresponding centerlines of the dark fringes (Fig. 3b) were obtained using the steps outlined above. Note that the fringes outside the blister were removed as they did not change during pressurization and did not affect the deflection of the membrane. Ideally, the deformation of the blister should be axisymmetric. The irregularity here was most likely due to variations in the membrane thickness. This can also be seen in the fringes outside the blister (Fig. 3a) where the flat substrate, by itself, would only generate straight fringes. The visibility of the delamination front in the interferograms allowed the blister height and its diameter to be measured simultaneously.

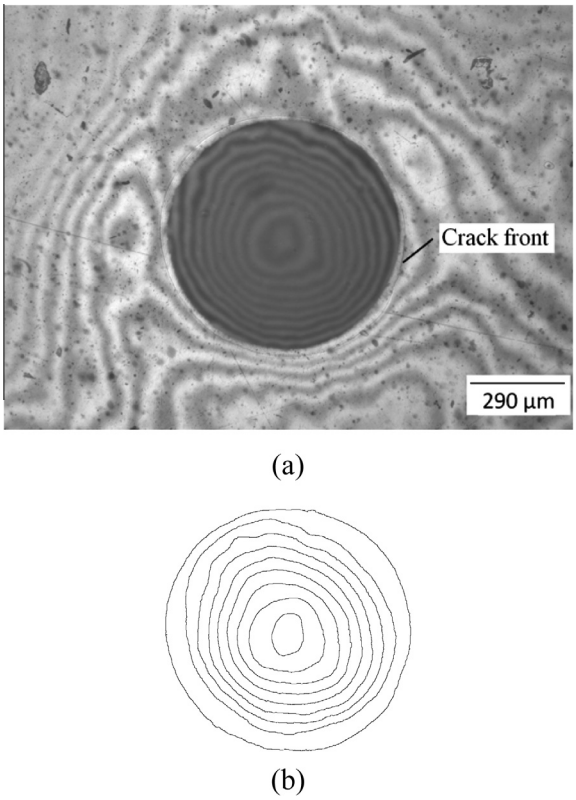

Fig. 3 – (a) An interferogram of a photoresist blister at 88.3 kPa. (b) The centerlines of the dark fringes. Background fringes have been eliminated in (b).

3. Modeling and analysis

In this section, two sets of analysis are presented for the pressurized blister. The first one is by a simple plate model assuming a fully clamped boundary condition at the delamination front and no residual stress. This analysis roughly captured the deflection profiles of the blister except near the delamination front. The energy release rate was estimated based on this analysis using the measured blister height and its diameter. However, the baking process during sample preparation likely introduced a residual stress, and the adhesive interactions near the delamination front were not strong enough to impose a fully clamped boundary condition. Therefore, a modified analysis was proposed to take into account the effects of the residual stress and some edge rotation with a relaxed boundary condition. In both analyses, the films were treated as isotropic, linearly elastic and homogeneous plates; the latter assumption was justified for graphene/photoresist bilayer as the photoresist was much thicker than graphene (see Appendix). The central deflection of the film was always less than a quarter of its thickness (t) in experiments, which justified the use of the linear elastic plate model for the data analysis.

In the simple plate model [27], the relationship between the pressure and central deflection of an elastic plate with Young's modulus E and Poisson's ratio ν is

$$h = \frac{pa^4}{64D} \tag{1}$$

where p, $D = \frac{Et^3}{12(1-\nu^2)}$, h, and a are the pressure, bending stiffness, central deflection and blister radius, respectively. The deflection profile of the circular blister is

$$w = \frac{pa^4}{64D}\left(1 - \frac{r^2}{a^2}\right)^2 \tag{2}$$

where r is the distance from center of the blister. The energy release rate for delamination of the membrane from the substrate can be obtained [28] as

$$G = \frac{32Dh^2}{a^4} \tag{3}$$

The derivation of the second analysis is more involved, and is developed in the Appendix. Here we only present the final results. The central deflection and the profile of the blister are

$$h = \frac{pa^2}{4\sigma_0 t} - C_1\sqrt{\frac{D}{\sigma_0 t}}\left[I_0\left(a\sqrt{\frac{\sigma_0 t}{D}}\right) - 1\right] \tag{4}$$

and

$$w\left(r\right) = \frac{p}{4\sigma_0 t}\left(a^2 - r^2\right) - C_1\sqrt{\frac{D}{\sigma_0 t}}\left[I_0\left(a\sqrt{\frac{\sigma_0 t}{D}}\right) - I_0\left(r\sqrt{\frac{\sigma_0 t}{D}}\right)\right] \tag{5}$$

where σ_0 is the residual stress and K_s is the rotational stiffness at the delamination front, and

$$C_1 = \frac{pa}{2\sigma_0 t}\left[\frac{\frac{K_s a}{D}+\nu+1}{\left(\frac{K_s a}{D}+\nu-1\right)I_1\left(a\sqrt{\frac{\sigma_0 t}{D}}\right)+a\sqrt{\frac{\sigma_0 t}{D}}I_0\left(a\sqrt{\frac{\sigma_0 t}{D}}\right)}\right] \quad (6)$$

with I_0 and I_1 being the modified Bessel functions of the first kind. It can be shown that, for $K_s \to \infty$ and $\sigma_0 \to 0$, Eqs. (4) and (5) recover the simple solution in Eqs. (1) and (2), respectively. The energy release rate is calculated by substituting (A.15) into (A.16), which is too long to be included here.

4. Results and discussion

In this section, results from two regimes of response are presented. Mechanical properties of the membranes were first extracted from the variation of pressure with the central deflection of the blister prior to delamination. Delamination resistance curves were then extracted during stable delamination based on the measurements and the analysis described in Sections 2 and 3.

An accurate measurement of the membrane thickness is fundamental to the analysis of the blister response, because of its cubed contribution to the bending stiffness. As indicated earlier, the thickness of each membrane was measured by placing them on a glass slide and scanning them with the profilometer. Fig. 4 is the result of such a procedure for the photoresist and graphene/photoresist membranes. The membrane thickness is the height of the step. Neglecting edge effects due to the cutting process, the average thickness was 33.2 ± 0.6 μm in both cases.

The pressure *vs.* central deflection response (Fig. 5) was obtained by counting the fringes (Fig. 3) as they crossed the center of the membrane while the pressure was increased. The discreteness of the height data is due to the digital nature of the fringes; the height was determined by the fringe number, increasing by 275 nm every time a new fringe crosses a particular location. The uncertainty in pressure measurements was within the size of the symbols. This data, along with the results of the simple and modified plate analyses are plotted together in Fig. 5. Two regimes can be detected. Before the kink, the blister bulged without delamination at the interface, and the central deflection increased linearly with the pressure. After the kink, the blister diameter increased as the membrane was delaminated from the substrate with a nearly circular delamination front, leading to a nonlinear response with a lower effective stiffness of the blister depending on the delamination growth. The initial linear response is quite different from the cubic one that is expected from membrane behavior [18]. This is due to the fact that the central deflections of the blister were considerably smaller than the film thickness $[(t/h)^2 \gg 1]$ in our experiments.

With the measured blister radius *a*, it was possible to fit the measured slope for pressure *vs.* central deflection by selecting the reduced modulus $\frac{E}{1-\nu^2}$ of the membrane in the simple plate analysis. Prior to delamination, the photoresist membrane yielded a slope $\frac{p}{h} = \frac{64D}{a^4} = 35.2$ GPa/m. With a thickness of 32.4 μm and a diameter of 0.797 mm, the reduced modulus was then 4.89 ± 0.12 GPa. Assuming Poisson's ratio of 0.3,

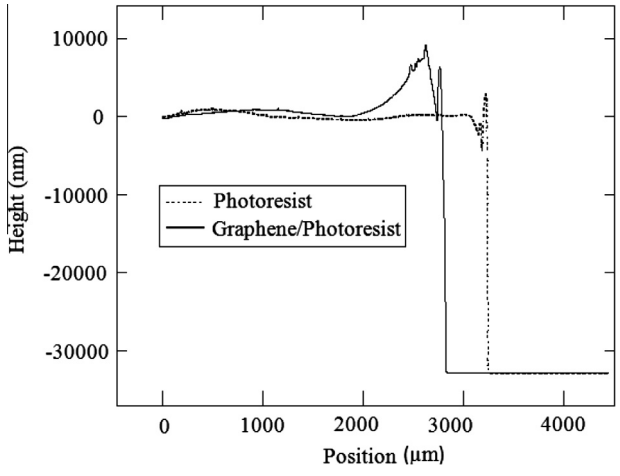

Fig. 4 – Profilometer scans of graphene/photoresist and photoresist samples. The average thickness is approximately 33.2 μm.

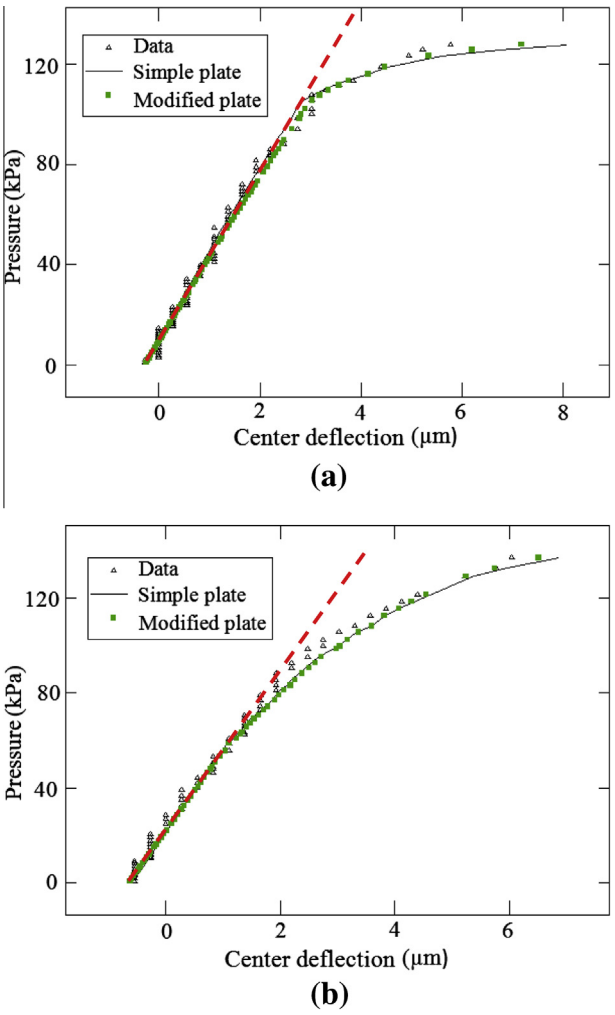

Fig. 5 – The variation of pressure with central displacement for (a) photoresist membrane and (b) graphene/photoresist membrane. (A color version of this figure can be viewed online.)

the Young's modulus of the photoresist is 4.45 ± 0.11 GPa. This result is in good agreement with existing data for similar photoresists [29,30]. Carrying out the same analysis on the membrane with graphene and photoresist yielded a reduced modulus of 4.54 GPa. The similarity of the values of reduced moduli for the two cases indicates that the presence of graphene did not change the stiffness of the membrane noticeably, which is not surprising since the in-plane stiffness of the photoresist membrane was about 400 times of the graphene (i.e., $E^p t >> E^g_{2D}$). For both types of the blister, the simple plate model agrees well with the measured data up until the last few points, where the model overestimates the deflection. The reason for the discrepancy is not clear, but the blister did become slightly oval with a minor to major axis ratio less than 1 but always greater than 0.9. Although the average radius was used in the modeling, there is still room for uncertainty as the radius effects height to the fourth power.

In preparation for obtaining bulge profiles at various pressure levels, the centerlines of the dark fringes were converted to three dimensional surfaces (Fig. 6) by interpolating between centerlines using the CFTOOL routine in MATLAB. Once these had been obtained, the deflected surface at zero pressure was taken to be the reference state and was subtracted from the surface topographies at all subsequent pressure levels to reveal the corresponding deflection. For comparison, radial profiles predicted from the simple and modified plate models were plotted as a function of pressure level (Fig. 7). The lines in Fig. 7a represent Eq. (2), which was developed under zero residual stress and a fully clamped boundary condition. However, in the experiment, residual stress was present and there was a nonzero deflection slope $\left(\frac{dw}{dr} = \theta\right)$ at $r = a$. These resulted in the discrepancy between measured and predicted deflections from the simple plate model, especially near the delamination front. The modified plate model was proposed to resolve these issues. By choosing the appropriate combination of residual stress and rotational stiffness through a parametric study, a better fit to the measured profiles was achieved (Fig. 7b). Using the same parameters, the center deflection *vs.* pressure response by the modified plate model shows no significant difference from the simple plate model (Fig. 5).

Examples of the delamination growth histories of specimens with photoresist and copper and photoresist, graphene and copper are shown in Fig. 8a and b, respectively. It can be seen that delamination accelerated gradually until the growth became unstable and the films blew off. The filled points in each case corresponded to steady-state behavior in the

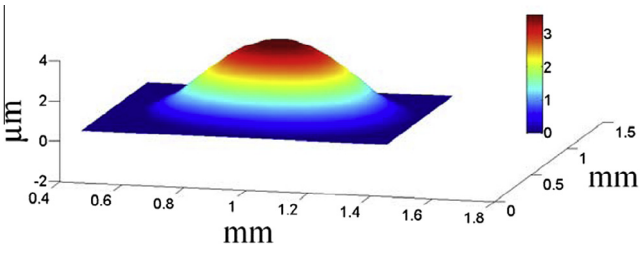

Fig. 6 – 3D profile of a blister at a pressure of 115 kPa. The deformation is with respect to the initial shape, a concave surface. (A color version of this figure can be viewed online.)

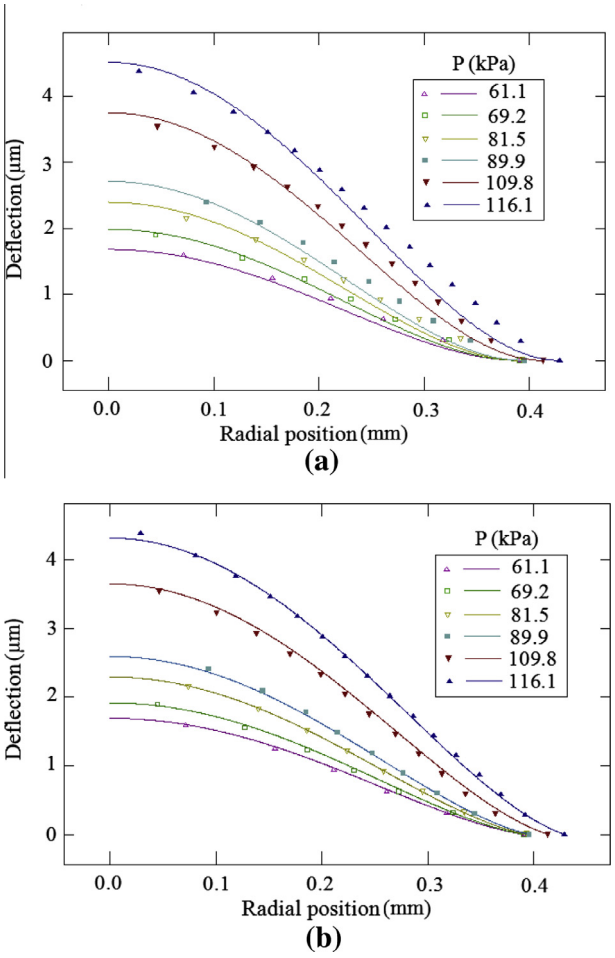

Fig. 7 – Profiles of a photoresist blister under varying pressures. Points are measured data. Lines are calculated from (a) simple and (b) modified plate models with $K_s = 0.32$ N and $\varepsilon_0 = 0.2\%$. (A color version of this figure can be viewed online.)

resistance curves (Fig. 9). In this regime, the delamination rates were 0.7 and 0.4 μm/s, respectively, for the photoresist/copper and graphene/copper interfaces.

The deflection profiles (Fig. 7) and the delamination growth data (Fig. 8) were the basis for determining delamination resistance curves (Fig. 9) that represented the adhesive interactions of the photoresist/copper (Fig. 9a and c) and graphene/copper (Fig. 9b and d) interfaces. In cases where an interface is completely brittle, its resistance curve is a step function which initiates at the origin and jumps to the toughness Γ_c of the interface. In other words, as soon as the energy release rate being provided by the pressure reaches Γ_c, the crack propagates and the energy release rate remains constant ($G = \Gamma_c$). For realistic interfaces, the step function is replaced by a gradually increasing resistance to delamination, which eventually reaches a steady state value Γ_{ss}, as the delamination proceeds with a constant energy release rate ($G = \Gamma_{ss}$). In the simple plate model, the energy release rate is calculated from Eq. (3), using the measured blister radius a and central deflection h along with the bending stiffness D obtained from the slope of the pressure *vs.* central deflection

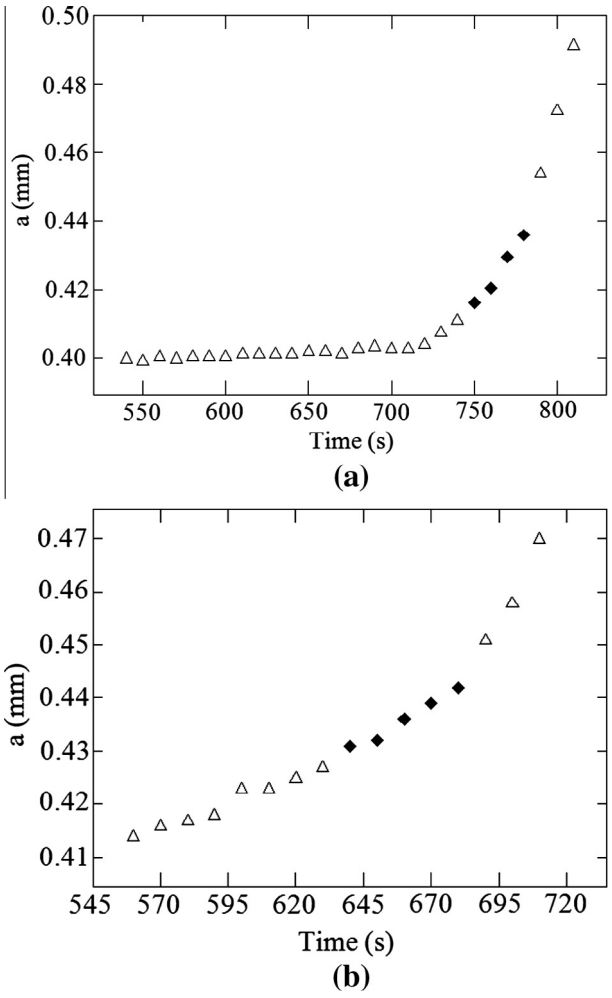

Fig. 8 – Crack growth histories for (a) photoresist/copper and (b) graphene/copper.

response (Fig. 5). Fig. 9a and b are the resistance curves for three photoresist/copper interfaces and four graphene/copper interfaces, respectively, each from different specimens. In all the cases, the resistance curves rose quite sharply from the initiation toughness ($G = \Gamma_0$) before reaching a steady state regime ($G = \Gamma_{ss}$), which then transitioned to unstable growth, represented by the last data point. This was taken to be the interfacial toughness of each particular specimen. The initiation toughness (Γ_0) of each interface was similar, ranging from 0.03 to 0.07 J/m^2 for the photoresist/copper interface and 0.02 to 0.08 J/m^2 for the graphene/copper interface. The corresponding average values for the steady state toughness (Γ_{ss}) obtained from all the specimens were 0.264 ± 0.013 and 0.341 ± 0.024 J/m^2, respectively, which are lower than the values for adhesive energy reported previously [9,29]. The blister was blown off shortly after the plateau was reached, most likely due to some compliance in the pressurization system. The amount of delamination growth that was required to achieve a steady state was approximately 50 μm in both cases. The total growth was approximately 100 μm before the blister became unstable.

Using the parameters determined in Fig. 7b, the energy release rate was also determined from the modified plate model with the effects of residual stress and rotational stiffness at the delamination front (see Appendix). Fig. 9c and d compare the resistance curves obtained from the modified plate model with those from the simple plate model, using one of the data sets for each interface. The two models yielded similar trends but the modified plate model resulted in higher energy release rates. The difference was largest just prior to onset of unstable growth. This is because the energy release rate from the modified plate model was calculated using the measured pressure and blister radius, as opposed to blister height and radius for the simple plate model. Since this model overestimated the blister height in this regime (Fig. 5), the calculated energy release rates using the measured pressure are higher than those using the measured height, which made the plateau in the resistance curve (Fig. 9c and d) disappear. Taking the last data point of the resistance curve as the closest approximation of the steady-state toughness, the modified plate model yielded toughness values of 0.465 ± 0.008 and 0.484 ± 0.007 J/m^2 for photoresist/copper and graphene/copper interfaces, respectively. The uncertainty was estimated by running the analysis with propagation of uncertainties in pressure, modulus and blister radius. As might be expected, these values of toughness are lower than the toughness of graphene being separated from seed copper [10]. They are in the same range as the values for graphene transferred to silicon [9]. Koenig et al. [9] noted that the measured adhesion energy of multi-layer graphene to silicon was less than that of monolayer graphene, likely due to a transition from conformal to non-conformal morphologies associated with the larger bending modulus of multilayer graphene [31]. Similar effects can be expected when graphene is backed by the much stiffer (based on tensile modulus times layer thickness) photoresist layer employed in this study. Moreover, it is interesting to note that, based on the fully clamped condition, the adhesive toughness of graphene transferred to copper was about 70 mJ/m^2 higher than that for photoresist alone. This suggests that the presence of graphene enhances the adhesion energy (in comparison to photoresist alone), which may be attributed to the close packing of carbon atoms in graphene. As noted before [32], the adhesion energy of van der Waals interactions is proportional to the number density of the atoms. At the same time, the modified analysis suggests that there is no significant difference between the adhesive toughness values of the two interfaces, which could suggest that there was no influence from the graphene. These issues clearly require further study. Finally, it should be noted that the fracture mode-mix (ratio of shear to tension) of the blisters in the present study is between −45° and −65° [20]. If there is any mode-mix dependence [33] for the interfacial fracture between graphene and copper, then further experiments would be required.

After the graphene/photoresist membrane had been blown off from the copper substrate, the graphene side of the membrane was inspected by Raman spectroscopy. This was to verify that the delamination occurred at graphene/copper interface rather than graphene/photoresist interface. The presence of graphene on the photoresist film before and after the blister test is indicated (Fig. 10) by the G and 2D peaks at 1583 and 2721 cm^{-1}, respectively. The D peak region (1350–1380 cm^{-1}), which is used to ascertain the quality of

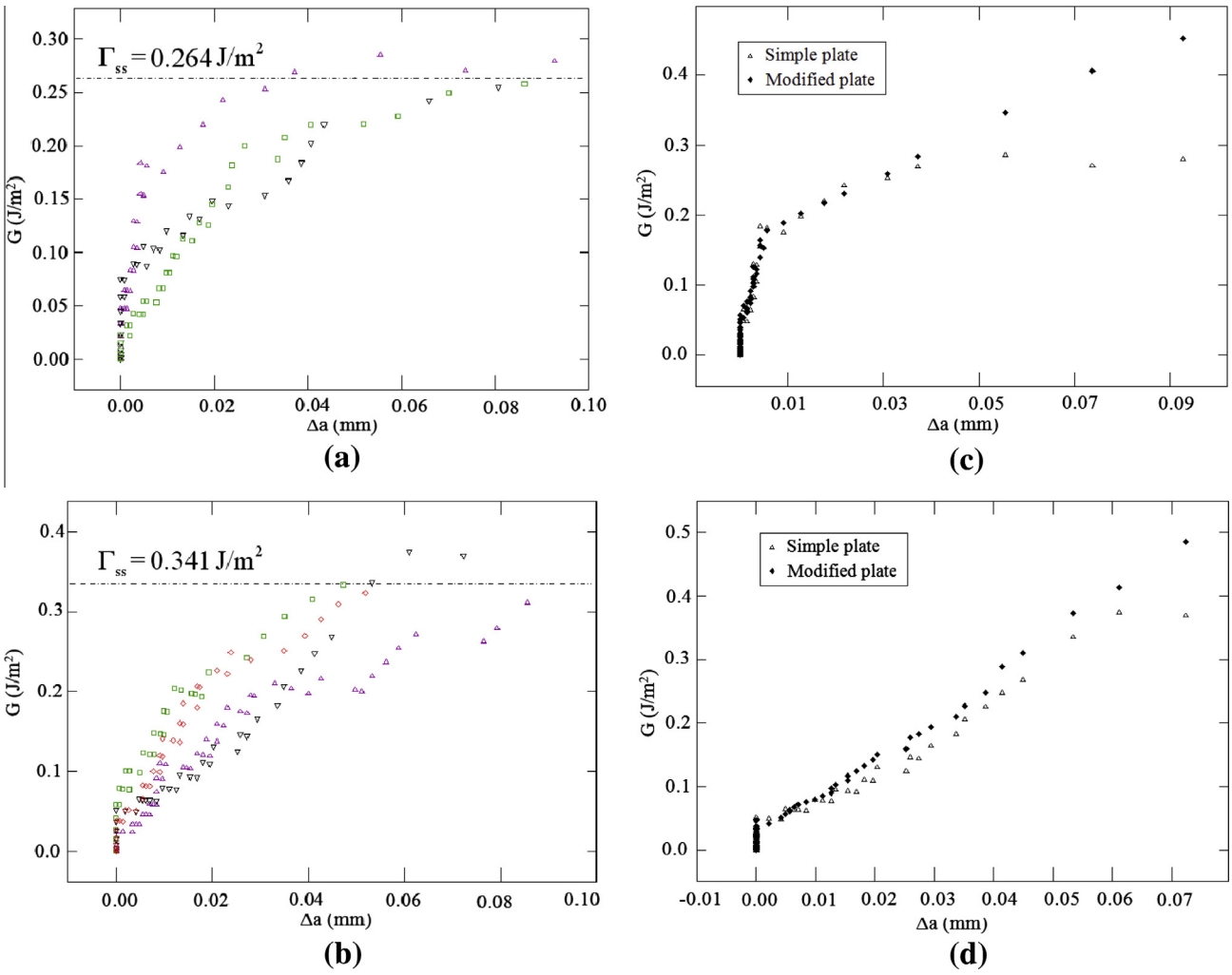

Fig. 9 – Resistance curves for (a) photoresist/copper and (b) graphene/copper interfaces based on the measurements and the simple plate model. A comparison of resistance curves from simple and modified plate models for (c) photoresist/copper and (d) graphene/copper interfaces, respectively. (A color version of this figure can be viewed online.)

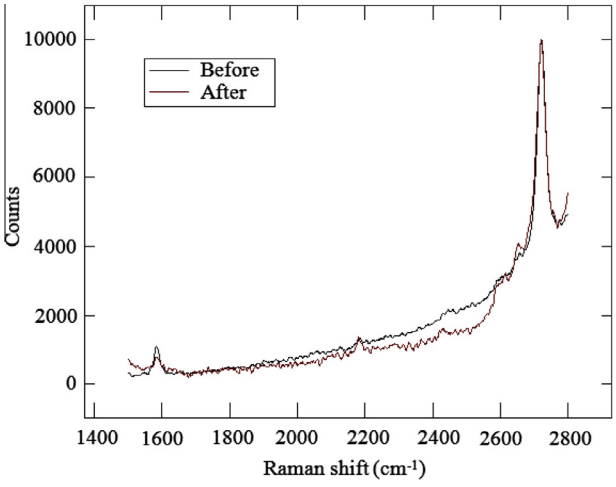

Fig. 10 – Raman spectra of the graphene side of the photoresist membrane before and after a blister test. (A color version of this figure can be viewed online.)

graphene, was present but was masked by contributions from the photoresist itself making it impossible to make a definitive assessment. The ratio of the peak intensities (I_G/I_{2D}) is 1:3 for high quality monolayer graphene [34] on silicon. The ratio obtained here was 1:12, which was an average of three spectra from two different specimens; each spectrum was itself an average of three runs. The lower intensity ratio is likely due to background noise produced by the photoresist, which is an epoxy that also contains sp^2 carbon bonding. Another possibility is contamination during the graphene transfer, most likely from residue of the PMMA [25] that was used in the transfer of the graphene to the copper substrate. This could indicate that the acetone did not completely remove the PMMA. Subsequent heating of the PMMA was not feasible in this case due to the potential for oxidization of the copper. Nonetheless, the intensity ratio of the G band to 2D band and the minimal D band indicate that the graphene was separated from the copper substrate with minimal defects.

5. Conclusions

This paper describes the development of a blister test for characterizing the interfacial adhesion of graphene that had been transferred to a polished copper surface over larger areas than have been previously considered. SU-8 2025 photoresist served as a backing layer, and its adhesion to copper was also studied for comparison. A simple plate model with zero residual stress and a fully clamped boundary was adopted to extract the mechanical behavior of each membrane and the interfacial toughness associated with their adhesion to copper. The blister profiles predicted by the simple model did not correspond to the measurements everywhere, with relatively large discrepancies near the delamination front. A modified plate model resolved this issue by accounting for the presence of residual stress and rotational stiffness at the delamination front. As a result, there was a difference in the calculated energy release rates for the resistance curves. The steady-state toughness or adhesion energy was obtained from the resistance curves; simple plate model yielded $0.264 \pm 0.013\ J/m^2$ and $0.341 \pm 0.024\ J/m^2$ for photoresist/copper and graphene/copper interfaces, respectively, whereas modified plate model yielded values of $0.44\ J/m^2$ and $0.51\ J/m^2$, emphasizing the need to account for residual stress effects and the rotational stiffness of the delamination front when relatively weak interactions are at play. The higher toughness values obtained by the modified analysis are in closer agreement with measurements of graphene interactions, albeit with other substrates. Raman spectroscopy was carried out to examine the delamination path for the copper/graphene/photoresist specimens, which confirmed delamination between copper and graphene over a large area.

Acknowledgements

The authors gratefully acknowledge partial financial support of this work by the National Science Foundation through Grant No. CMMI-1130261. This work is also based upon work supported in part by the National Science Foundation under Cooperative Agreement No. EEC-1160494. Any opinions, findings and conclusions or recommendations expressed in this material are those of the author(s) and do not necessarily reflect the views of the National Science Foundation.

Appendix A

Prior to pressurization, the strain components of the membrane are:

$$\varepsilon_r = \varepsilon_0, \quad \varepsilon_\theta = \varepsilon_0 \quad \text{and} \quad \varepsilon_{r\theta} = 0, \tag{A.1}$$

where ε_0 is the pre-strain. The radial and circumferential membrane forces are:

$$N_r = N_\theta = S\varepsilon_0, \tag{A.2}$$

where S is the biaxial in-plane stiffness of the membrane. The average residual stress is then $\sigma_0 = S\varepsilon_0/t$, where t is the membrane thickness.

Upon pressurization, the deflection profile of the circular blister is assumed to be axi-symmetric with $w = w(r)$. The curvature components are

$$\kappa_r = \frac{d^2w}{dr^2}, \quad \kappa_\theta = \frac{1}{r}\frac{dw}{dr} \quad \text{and} \quad \kappa_{r\theta} = 0. \tag{A.3}$$

The corresponding bending moments are

$$M_r = D\left(\frac{d^2w}{dr^2} + \frac{v}{r}\frac{dw}{dr}\right) \text{and} M_\theta = D\left(v\frac{d^2w}{dr^2} + \frac{1}{r}\frac{dw}{dr}\right) \tag{A.4}$$

where D is the bending stiffness and v is Poisson's ratio. Moment equilibrium yields the equation for the deflection of the membrane:

$$D\left(\frac{d^3w}{dr^3} + \frac{1}{r}\frac{d^2w}{dr^2} - \frac{1}{r^2}\frac{dw}{dr}\right) - \sigma_0 t\frac{dw}{dr} = \frac{1}{r}\int_0^r qrdr \tag{A.5}$$

where q is the lateral loading intensity. In the present study, the loading was a uniform pressure $q = p$ and the right hand side reduces to $pr/2$.

Because of symmetry, the boundary condition at center ($r = 0$) is $\theta = \frac{dw}{dr} = 0$. At the delamination front $r = a$, the deflection $w = 0$. In order to account for the possibility of rotation at the delamination front due to the nature of the interactions between the film and substrate, a spring-like boundary condition is assumed:

$$M_r = D\left(\frac{d^2w}{dr^2} + \frac{v}{r}\frac{dw}{dr}\right) = -K_s\frac{dw}{dr} \tag{A.6}$$

where K_s is the rotational stiffness of the delamination front. This indicates that, at the boundary ($r = a$), the radial moment is proportional to angle of rotation. When $K_s = 0$, the boundary condition becomes a simply-supported one while the fully-clamped condition corresponds to $K_s \to \infty$.

The solution to Eq. (A.5) can be developed by rewriting it in terms of the rotation $\theta = \frac{dw}{dr}$ as

$$\frac{d^2\theta}{dr^2} + \frac{1}{r}\frac{d\theta}{dr} - \left(\frac{1}{r^2} + \frac{\sigma_0 t}{D}\right)\theta = \frac{pr}{2D} \tag{A.7}$$

The angle of rotation is then obtained as

$$\theta(r) = C_1 I_1\left(r\sqrt{\frac{\sigma_0 t}{D}}\right) + C_2 K_1\left(r\sqrt{\frac{\sigma_0 t}{D}}\right) - \frac{pr}{2\sigma_0 t} \tag{A.8}$$

where $I_1(x)$ and $K_1(x)$ are modified Bessel functions of the first and second kinds, respectively. Applying the boundary condition at $r = 0$ leads to $C_2 = 0$, and the condition (A.6) at $r = a$ yields

$$C_1 = \frac{pa}{2\sigma_0 t}\left[\frac{\frac{K_s a}{D} + v + 1}{\left(\frac{K_s a}{D} + v - 1\right)I_1\left(a\sqrt{\frac{\sigma_0 t}{D}}\right) + a\sqrt{\frac{\sigma_0 t}{D}}I_0\left(a\sqrt{\frac{\sigma_0 t}{D}}\right)}\right] \tag{A.9}$$

The deflection is then obtained by integrating the angle of rotation so that

$$w = \frac{p}{4\sigma_0 t}\left(a^2 - r^2\right) - C_1\sqrt{\frac{D}{\sigma_0 t}}\left[I_0\left(a\sqrt{\frac{\sigma_0 t}{D}}\right) - I_0\left(r\sqrt{\frac{\sigma_0 t}{D}}\right)\right]. \tag{A.10}$$

The central deflection is thus

$$h = \frac{pa^2}{4\sigma_0 t} - C_1\sqrt{\frac{D}{\sigma_0 t}}\left[I_0\left(a\sqrt{\frac{\sigma_0 t}{D}}\right) - 1\right] \tag{A.11}$$

To obtain the energy release rate for advancing the delamination front, we calculate the total potential energy as follows. The strain energy of the membrane consists of two parts: one due to bending and the other one due to stretching. With the biaxial residual stress, the elastic stretching energy per unit area is approximately

$$U_s(r) = \frac{\sigma_0 t}{2}\left(\frac{dw}{dr}\right)^2 \tag{A.12}$$

The elastic bending energy per unit area is

$$U_b(r) = \frac{D}{2}\left(\left(\frac{d^2w}{dr^2}\right)^2 + \frac{1}{r^2}\left(\frac{dw}{dr}\right)^2 + \frac{2v}{r}\frac{dw}{dr}\frac{d^2w}{dr^2}\right) \tag{A.13}$$

In addition, the potential energy due to the rotational spring-like condition at the delamination front (per unit length) is

$$U_k = \frac{1}{2}K_s\left(\frac{dw}{dr}\right)^2\Big|_{r=a} \tag{A.14}$$

The total potential energy of the pressurized blister is then

$$\begin{aligned}\Pi(a,p) &= 2\pi\int_0^a [U_s(r)+U_b(r)]rdr + 2\pi a U_k - 2\pi p\int_0^a w(r)rdr \\ &= -\pi p\int_0^a w(r)rdr \\ &= -\frac{\pi p^2 a^4}{16\sigma_0 t} - \frac{\pi D p^2 a^2}{2(\sigma_0 t)^2}\frac{\left(\frac{K_s a}{D}+v+1\right)\left[I_1\left(a\sqrt{\frac{\sigma_0 t}{D}}\right) - \frac{a}{2}\sqrt{\frac{\sigma_0 t}{D}}I_0\left(a\sqrt{\frac{\sigma_0 t}{D}}\right)\right]}{\left(\frac{K_s a}{D}+v-1\right)I_1\left(a\sqrt{\frac{\sigma_0 t}{D}}\right) + a\sqrt{\frac{\sigma_0 t}{D}}I_0\left(a\sqrt{\frac{\sigma_0 t}{D}}\right)}\end{aligned} \tag{A.15}$$

The energy release rate for delamination is obtained as a function of the blister radius and the pressure as

$$G(a,p) = -\frac{1}{2\pi a}\left(\frac{\partial\Pi(a,p)}{\partial a}\right) \tag{A.16}$$

For fully clamped boundary condition with $K_s \to \infty$, the potential energy becomes

$$\Pi(a,p) = -\frac{\pi p^2 a^4}{16\sigma_0 t} - \frac{\pi D p^2 a^2}{2(\sigma_0 t)^2}\left[1 - \frac{a\sqrt{\frac{\sigma_0 t}{D}}I_0\left(a\sqrt{\frac{\sigma_0 t}{D}}\right)}{2I_1\left(a\sqrt{\frac{\sigma_0 t}{D}}\right)}\right]. \tag{A.17}$$

Further when $\sigma_0 \to 0$, the potential energy reduces to

$$\Pi(a,p) = -\frac{\pi p^2 a^6}{384D}. \tag{A.18}$$

Substitution of (A.18) into (A.16) recovers the simple solution in Eq. (3) for the energy release rate with zero residual stress and fully clamped boundary condition.

The membrane with photoresist and graphene can be considered as a bilayer composite plate of total thickness t. The effective biaxial in-plane stiffness of the composite is

$$S = \frac{1}{1-v}\left(E^p t + E^g_{2D}\right) = \frac{E^p t}{1-v}(1+\lambda) \tag{A.19}$$

where E^p is Young's modulus of the photoresist, E^g_{2D} is the two-dimensional Young's modulus of graphene [4], and $\lambda = \frac{E^g_{2D}}{E^p t}$. Because the graphene monolayer is much thinner than the photoresist, the overall Poisson's ratio is approximately that of the photoresist alone. Similarly, the effective bending stiffness of the composite membrane is approximately

$$D = \frac{E^p t^3}{12(1-v^2)}\frac{1+4\lambda}{1+\lambda}. \tag{A.20}$$

For our experiments, $E^p t >> E^g_{2D}$ and $\lambda \to 0$. Hence, we have $S \approx \frac{E^p t}{1-v}$ and $D \approx \frac{E^p t^3}{12(1-v^2)}$, implying that we can use the in-plane and bending stiffness of the photoresist alone for the composite membrane.

REFERENCES

[1] Lee C, Wei XD, Kysar JW, Hone J. Measurement of the elastic properties and intrinsic strength of monolayer graphene. Science 2008;321(5887):385–8.

[2] Lin YM, Dimitrakopoulos C, Jenkins KA, Farmer DB, Chiu HY, Grill A, et al. 100 GHz transistors from wafer-scale epitaxial graphene. Science 2010;327(5966). 662-662.

[3] Bae S, Kim H, Lee Y, Xu XF, Park JS, Zheng Y, et al. Roll-to-roll production of 30 in. graphene films for transparent electrodes. Nat Nanotechnol 2010;5(8):574–8.

[4] Li XS, Cai WW, An JH, Kim S, Nah J, Yang DX, et al. Large-area synthesis of high-quality and uniform graphene films on copper foils. Science 2009;324(5932):1312–4.

[5] Kim KS, Zhao Y, Jang H, Lee SY, Kim JM, Kim KS, et al. Large-scale pattern growth of graphene films for stretchable transparent electrodes. Nature 2009;457(7230):706–10.

[6] Sutter PW, Flege JI, Sutter EA. Epitaxial graphene on ruthenium. Nat Mater 2008;7(5):406–11.

[7] Batzill M. The surface science of graphene: metal interfaces, CVD synthesis, nanoribbons, chemical modifications, and defects. Surf Sci Rep 2012;67(3–4):83–115.

[8] Zong Z, Chen CL, Dokmeci MR, Wan KT. Direct measurement of graphene adhesion on silicon surface by intercalation of nanoparticles. J Appl Phys 2010;107(2):026104.

[9] Koenig SP, Boddeti NG, Dunn ML, Bunch JS. Ultrastrong adhesion of graphene membranes. Nat Nanotechnol 2011;6:543–6.

[10] Yoon T, Shin WC, Kim TY, Mun JH, Kim TS, Cho BJ. Direct measurement of adhesion energy of monolayer graphene as-grown on copper and its application to renewable transfer process. Nano Lett 2012;12(3):1448–52.

[11] Hinkley JA. A blister test for adhesion of polymer films to SiO_2. J Adhes 1983;16:115–25.

[12] Gent AN, Lewandowski LH. Blow-off pressures for adhering layers. J Appl Polym Sci 1987;33:1567–77.

[13] Liechti KM, Hanson E. Nonlinear effects in mixed-mode delaminations. Int J Fract 1988;36:199–217.

[14] Liechti KM, Shirani A. Large scale yielding in blister specimens. Int J Fract 1994;67:21–36.

[15] Allen MG, Mehregany M, Howe RT, Senturia SD. Microfabricated structures for the *in situ* measurement of residual stress, young's modulus, and ultimate strain of thin films. Appl Phys Lett 1987;51:241–3.

[16] Allen MG, Senturia SD. Analysis of critical debonding pressures of stressed thin films in the blister test. J Adhes 1988;25:303–15.

[17] Allen MG, Senturia SD. Application of the island blister test for thin film adhesion measurement. J Adhes 1989;29:219–31.

[18] Hohlfelder RJ, Luo HH, Vlassak JJ, Chidsey CED, Nix WD. Measuring interfacial fracture toughness with the blister test. Mater Res Soc Symp Proc 1997;436:115–20.

[19] Yahiaoui R, Danaie K, Petitgrand S, Bosseboeuf A. An automated interferometric system for bulge and blister test measurements of micromachined membranes. Proc SPIE 2001;4400:160–9.

[20] Jensen HM. Analysis of mode mixity in blister tests. Int J Fract 1998;94:79–88.
[21] Liechti KM, Shirani A, Dillingham RG, Boerio FJ, Weaver SM. Cohesive zone models of polyimide/aluminum interphases. J Adhes 2000;73:259–97.
[22] Shirani A, Liechti KM. A calibrated fracture process zone model for thin film blistering. Int J Fract 1998;93(1–4):281–314.
[23] Wang P, Gao W, Cao Z, Liechti KM, Huang R. Numerical analysis of circular graphene bubbles. J Appl Mech 2013;80:040905.
[24] Tao L, Lee J, Chou H, Holt M, Ruoff RS, Akinwande D. Synthesis of high quality monolayer graphene at reduced temperature on hydrogen-enriched evaporated copper (111) films. ACS Nano 2012;6(3):2319–25.
[25] Li XS, Zhu YW, Cai WW, Borysiak M, Han BY, Chen D, et al. Transfer of large-area graphene films for high-performance transparent conductive electrodes. Nano Lett 2009;9(12):4359–63.
[26] Suk JW, Kitt A, Magnuson CW, Hao Y, Ahmed S, An J, et al. Transfer of CVD-grown monolayer graphene onto arbitrary substrates. ACS Nano 2011;5(9):6916–24.
[27] Timoshenko SP, Woinowsky-Krieger S. Theory of plates and shells. 2nd ed. New York: McGraw-Hill; 1987. p. 93.
[28] Kanninen MF, Popelar CH. Advanced fracture mechanics. Oxford, UK: Oxford University Press; 1985. p. 375.
[29] Goyal S, Srinivasan K, Subbarayan G, Siegmund T. A non-contact, thermally-driven buckling delamination test to measure interfacial fracture toughness of thin film systems. Thin Solid Films 2010;518(8):2056–64.
[30] Al-Halhouji AT, Kampen I, Krah T, Buettgenbach S. Nanoindentation testing of SU-8 photoresist mechanical properties. Microelectron Eng 2008;85(5–6):942–4.
[31] Gao W, Huang R. Effect of surface roughness on adhesion of graphene membranes. J Phys D Appl Phys 2011;44(45):452001.
[32] Aitken ZH, Huang R. Effects of mismatch strain and substrate surface corrugation on morphology of supported monolayer graphene. J Appl Phys 2010;107:123531.
[33] Chai YS, Liechti KM. Asymmetric shielding in interfacial fracture under in-plane shear. J Appl Mech 1992;59:295–304.
[34] Ferrari AC, Meyer JC, Scardaci V, Casiraghi C, Lazzeri M, Mauri F, et al. Raman spectrum of graphene and graphene layers. Phys Rev Lett 2006;97(18):187401.